University of Wisconsin-January 2014 DERC Report

Experimental Investigation of Piston Heat Transfer in a Light Duty Engine

Eric Gingrich

Experimental Setup

Single-Cylinder Engine Laboratory

Experiments were conducted in a light-duty single-cylinder engine based on the General Motors/Fiat JTD 1.9L four-cylinder diesel engine. A stock four cylinder head was installed atop a single cylinder block. Valves for cylinder #2 were activated by the dual overhead cams. The valvetrain for the remaining three cylinders was deactivated by removing the valve rocker arms. Table 1 (adapted from Dempsey et al. [1]) shows the specifications for the engine.

Table 1.Engine specifications

Engine Geometry	
Base Engine	GM 1.9L Diesel
Compression Ratio	16.3
Displacement (Liters)	0.477
Stroke (mm)	90.4
Bore (mm)	82
Intake Valve Closing	-132° aTDC
Exhaust Valve Opening	112° aTDC
Swirl Ratio	1.5 -4.8
Piston Bowl Type	Stock (Re-entrant)
Port Fuel Injectors	
Included Spray Angle	20°
Injection Pressure (bar)	2 to 10
Rated Flow (cc/sec)	< 10
Bosch Common Rail Injector	
Number of Holes	7
Hole Diameter (mm)	0.14
Included Spray Angle	155°
Injection Pressure (bar)	250 to 1000 bar

The research engine is equipped with a choked orifice air flow metering system that is fed with building air. An electrical heater is used to increase the temperature of the air. The air system includes an exhaust gas recirculation loop (EGR) to provide dilution when necessary. The EGR-air mixture enters a heated intake surge tank to dampen wave dynamics. Two port fuel injectors (PFI), plumbed with separate fuel systems, deliver up to two different fuels to create the premixed charge. There are two swirl-control vanes that provide an adjustable swirl ratio between 1.5 and 4.8. The engine has an additional high pressure common rail fuel injector that allows for direct injection of a third fuel. After leaving the engine the exhaust enters a surge tank to dampen wave dynamics and enhance mixing. Small samples of the exhaust gas are acquired by an

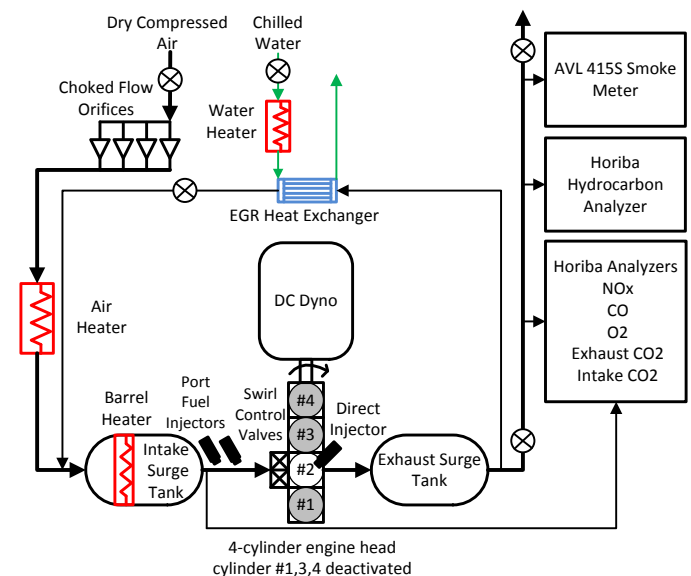AVL 415S smoke meter and Horiba gas analyzers. Figure 1 shows the experimental laboratory schematically.

Figure 1. Experimental engine layout

The engine is controlled with National Instruments LabView system. The fuel injection systems are controlled by Drivven PCI controller cards. The system controls and records, engine airflow, emissions data, EGR valve, pressures, low speed temperatures, and other critical engine parameters. The fuel mass flow rates were measured separately by Coriolis flow meters. A shaft encoder with 1440 pulses per revolution was used to trigger the high speed data acquisition system. In-cylinder pressure was measured with a Kistler 6125A pressure transducer in series with a Kistler 5010 charge amplifier.

Wireless Telemetry System

Temperature data were transferred from the piston through a IR Telemetrics model 3051 microwave transmitter system. The electromotive force (EMF) generated at each thermocouple was converted to a frequency modulated square wave over the range of 10-50kHz. A voltage-controlled oscillator then converts the square wave into a microwave signal. The microwave signal is broadcast into the crankcase where four receiving antennas are mounted. The signal is amplified, converted back to a modulated square wave, downconverted, then the original EMF is recorded. The signal conversion process induces a degree of filtering but the advertised

Report Documentation Page

Form Approved
OMB No. 0704-0188

1. REPORT DATE	2. REPORT TYPE	3. DATES COVERED
30 JAN 2014	**Journal Articles**	**06-01-2014 to 13-01-2014**

4. TITLE AND SUBTITLE	5a. CONTRACT NUMBER
Experimental Investigation of Piston Heat Transfer in a Light Duty Engine	5b. GRANT NUMBER
	5c. PROGRAM ELEMENT NUMBER

6. AUTHOR(S)	5d. PROJECT NUMBER
Eric Gingrich	5e. TASK NUMBER
	5f. WORK UNIT NUMBER

7. PERFORMING ORGANIZATION NAME(S) AND ADDRESS(ES)	8. PERFORMING ORGANIZATION REPORT NUMBER
U.S. Army TARDEC,6501 East Eleven Mile Rd,Warren,Mi,48397-5000	**#24383**

9. SPONSORING/MONITORING AGENCY NAME(S) AND ADDRESS(ES)	10. SPONSOR/MONITOR'S ACRONYM(S)
U.S. Army TARDEC, 6501 East Eleven Mile Rd, Warren, Mi, 48397-5000	**TARDEC**
	11. SPONSOR/MONITOR'S REPORT NUMBER(S) **#24383**

12. DISTRIBUTION/AVAILABILITY STATEMENT
Approved for public release; distribution unlimited

13. SUPPLEMENTARY NOTES
University of Wisconsin January 2014 DERC Report

14. ABSTRACT
Experiments were conducted in a light-duty single-cylinder engine based on the General Motors/Fiat JTD 1.9L four-cylinder diesel engine. A stock four cylinder head was installed atop a single cylinder block. Valves for cylinder #2 were activated by the dual overhead cams. The valvetrain for the remaining three cylinders was deactivated by removing the valve rocker arms.

15. SUBJECT TERMS

16. SECURITY CLASSIFICATION OF:			17. LIMITATION OF ABSTRACT	18. NUMBER OF PAGES	19a. NAME OF RESPONSIBLE PERSON
a. REPORT **unclassified**	b. ABSTRACT **unclassified**	c. THIS PAGE **unclassified**	**Public Release**	**10**	

Standard Form 298 (Rev. 8-98)
Prescribed by ANSI Std Z39-18

bandwidth of the system is 10kHz [2]. Similar systems have been used by other researchers[3, 4].

The microwave transmitter only broadcasts data from one channel at a time; it cycles though the seven different channels (+1 marker channel). Thermocouple data was only recorded on two channels due to sensor failure (which will be discussed later). The transmitter was configured to broadcast each channel for 0.5 seconds independent of engine speed. At higher engine speed more engines cycles will be transmitted than at slower engine speeds. The data streaming off the engine is collected for a fixed amount of time and the data are saved to a local computer.

The electronics associated with the wireless telemetry system are powered by an inductive power supply. An exciter coil, mounted on the underside of the piston liner, is powered by an inductive power supply. When the piston is near bottom dead center (BDC) a secondary coil that is mounted on the piston skirt interfaces with the exciter coil allowing power to transfer inductively. Capacitors and other electronics store enough energy to power the piston though the entire engine cycle.
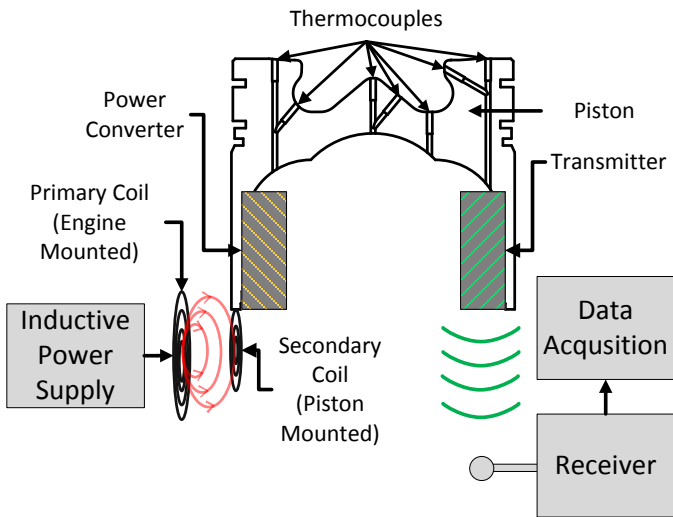

Figure 2. Wireless Telemetry System

Thermocouple Specifications

Seven fast-response coaxial thermocouples were installed in the piston crown to measure dynamic surface temperature. Thermocouple data was only recorded on two channels due to sensor failure. Coaxial thermocouples have been used in a variety of applications. The sensor can survive harsh environments including the high temperatures, pressures and accelerations typically encountered in an engine. Thermocouples with both plated and slivered junctions were installed in the piston. Surface thermocouples can either have a plated junction formed by plating the surface of the probe [5], or a sliver junction, formed by cold-weld slivers of one material onto the next. Both types of probes were utilized in this work. The thermocouples were J-type, with the center wire consisting of Constantan and the outer tube of Iron. The thermocouples, Medtherm part numbers TCS-061-JU-0.25 and TCS-061-JU-0.25-CR were claimed to have a time constant of one

microsecond for the plated junction probes and a ten microsecond time constant for the sliver junction probes [6].

Table 2 and Figure 3 list and depict the location of the thermocouples mounted in the piston. All the thermocouples were mounted in a plane perpendicular to the wrist pin. Figure 4 shows a top view of the piston.

Upon engine startup thermocouples 4,5, and 6 registered no signal. A problem with the thermocouples, wiring or telemetry system did not allow any data to be collected on these channels. Throughout testing thermocouples, 1 and 2 reported data intermittingly. It is believed that deposit buildup may have caused these issues. Thermocouples 3 and 7 provided repeatable data throughout the duration of testing.

Table 2 Thermocouple Locations

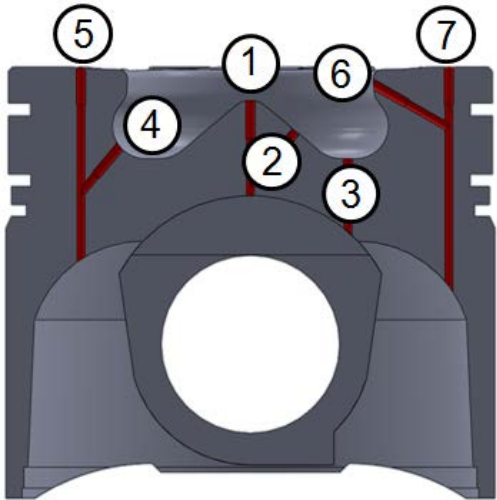| Number	R (in)	Z (in)	Angle (deg)	Plating
1	0	-0.217	VERTICAL	Chromium
2	0.3	-0.425	39.6	Chromium
3	0.644	-0.605	VERTICAL	Chromium
4	-0.861	-0.527	40	None
5	0.813	-0.113	60	None
6	-1.118	-0.006	VERTICAL	None
7	1.31	0	VERTICAL	Chromium

Figure 3. Piston cross-section showing fast response surface thermocouples

Figure 4 Piston top view showing fast response surface thermocouples

Temperature Data Processing

Data Reduction

The temperature data recorded by the wireless telemetry system included spurious spikes that needed to be removed before the heat flux could be calculated. The spikes in the data were caused by the wireless telemetry process. When the piston-mounted transmitter has direct line of sight with one of the receiving antennas, the transfer of data from the piston to the antennas is nearly 100%. During times of the engine cycle when the transmitter does not have good visibility (i.e. near TDC) with the antennas, the transmission efficiency is degraded. Figure 5 shows the raw temperature data as recorded by the vendor software. Useful temperature data are buried among the non-reasonable points that include negative values and values beyond the melting point of the piston.
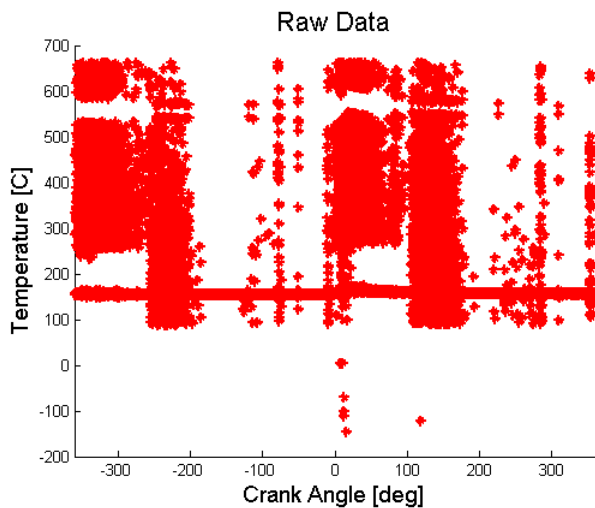

Figure 5 Temperature data including spurious spikes before processing on a sample data set

Spurious raw data were eliminated by applying the generalized extreme Studentized deviate (ESD) test at each crank angle. The ESD test is used to detect one or more outliers in a data set that approximately follows a normal distribution [7]. This statistical tool is preferred over other tests because it does not require that the number of outliers be predefined before the test is run [8]. Typically 5% of all data was removed by this procedure. In the region between -20degATDC and 20degATDC, approximately 25% of the data were removed. Figure 6 shows temperature data after the ESD test was applied.
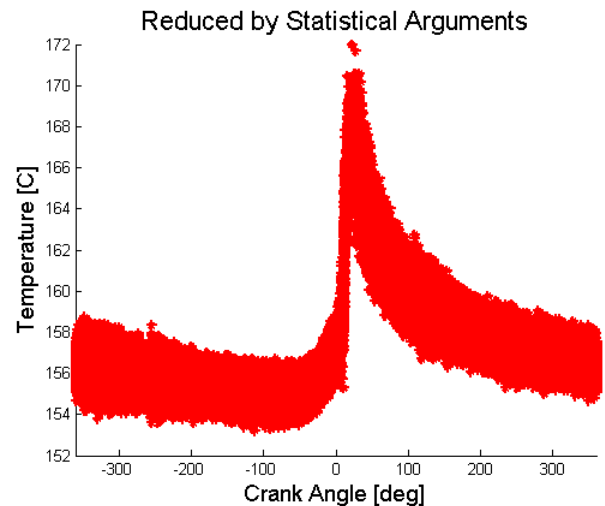

Figure 6 Temperature data after application of ESD outlier elimination on a sample data set

After the ESD test was applied the remaining data were averaged at each crank angle degree. Figure 7 shows the resulting temperature plot
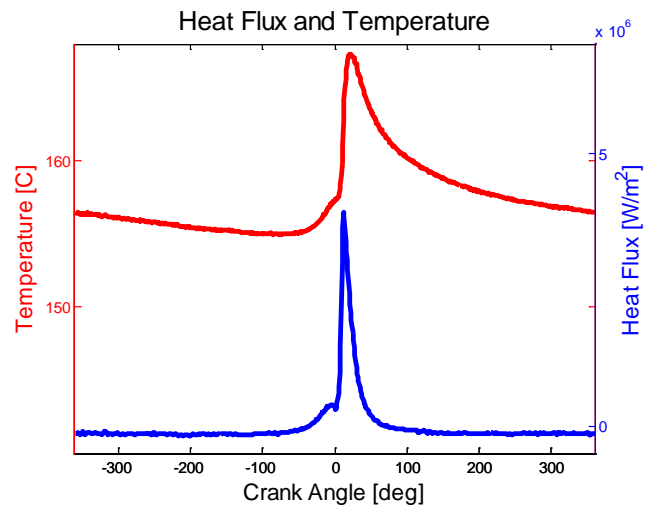

Figure 7 Full cycle temperature and heat flux data

Instantaneous Heat Flux Calculation

The surface heat flux of an internal combustion engine can be represented by two components: the steady-state and the transient response. The steady-state component is calculated from a time-averaged surface temperature measurement and a back-side thermocouple at a known depth beneath the surface. The transient component is calculated using a time-varying surface temperature measurement. The thermocouples used in this study only included surface thermocouples and therefore only the transient heat flux was calculated.

To calculate the surface heat flux a one-dimensional assumption must be made. A Fourier analysis is utilized to decompose the temperature data into frequency components. In Equation (1) The Fourier coefficients A_n and B_n are calculated by applying a Fast Fourier Transform. T_m is the mean surface temperature, n is harmonic number and ω is the angular velocity of the engine. The FFT method, as is it commonly known, has been used by other researchers to calculate surface heat flux in IC engines [9-11].

$$T(t) = T_m + \sum [A_n \cos(n\omega t) + B_n \sin(n\omega t)] \qquad (1)$$

Equation (2) is the periodic transient solution for the surface heat flux. All variables are known from the Fourier analysis with the exception of the thermal properties of the material, the conductivity, k, and the thermal diffusivity, α. The thermal properties used in this study will be discussed next.

$$\dot{q}_{trans} = k \sum_{n=1}^{N} \sqrt{\frac{n\omega}{2\alpha}} [(A_n + B_n)\cos(n\omega t) - (A_n - B_n)\sin(n\omega t)] \qquad (2)$$

To calculate heat flux thermal properties must be chosen. The J-type thermocouples used have Constantan as the inner wire and Iron as the outer tube. The piston is constructed from an aluminum alloy. But, the simplified one-dimensional analysis only allows for a single set of properties to be used.. Three-dimensional finite element analysis (FEA) has shown that the heat flux measurement most closely matches the input value when the material properties for the inner wire are used [12].

The thermal properties for Constantan were used in equation (2) to calculate the heat flux. For each case the time average surface temperature was used to calculate the conductivity and thermal diffusivity based on measurements made by Sasaki et al. [13]. The thermal properties are allowed to vary slightly to account for changes in operating conditions from run to run, but were held constant as temperature varies throughout the engine cycle. Figure 7 shows the full-cycle temperature and heat flux. The heat flux is relatively constant at a negative value through the intake and exhaust part of the cycle. This negative value is a result of only solving for the dynamic part of the heat flux solution. During the compression and expansion part of the cycle, the heat flux increases due to the increased gas temperature first due to compression, and then from the high-temperature combustion products.

To have an understanding of the total energy transfer, the transient heat flux was integrated over the closed part of the cycle from intake value closing (IVC) to exhaust value opening (EVO). This value is reported hereafter as the integrated heat flux.

Results and Discussion

Operating Conditions

The engine was operated at four different load and speed points (referred to hereafter by mode number) as listed in Table 3 using RCCI, HCCI, and CDC combustion strategies. The combustion phasing (CA50), gross IMEP, intake temperature, and intake pressure were matched for the different combustion regimes. Matching load and CA50 was thought to give the best comparison between the different regimes although this may mean a particular combustion regime was operating at a non-optimal point. Mode 2 was also used to conduct a parametric study of CA50 and swirl effects. The CA50 and swirl conditions run for these tests are listed in Table 4 and Table 5, respectively. Swirl was varied by adjusting the swirl-control vanes mounted on the intake ports of the engine.

Table 6 lists the different fuels used for the various combustion regimes. In order to control combustion phasing with HCCI two different fuels were injected using two port fuel injectors connected to different fuel systems. Gasoline, with a pump octane number (PON) of 91, was used in one PFI and a mixture of gasoline and n-heptane was used in the other PFI. N-heptane is an extremely reactive fuel that functioned to lower the octane number of the gasoline. Individual control of the two PFIs allowed the reactivity (octane number) of the mixture to be changed allowing CA50 to be set. CDC was operated using F76, which is a military specification diesel fuel having ignition quality and distillation curves similar to an ultra-low sulfur diesel (ULSD). During RCCI operation F76 was directly injected and 91PON gasoline was port injected.

Table 3 Engine operating conditions at different loads and speeds

	Mode 1	Mode 2	Mode 3	Mode 4
Speed (RPM)	1490	1900	2300	2300
IMEPg (bar)	4.2	5.7	5.7	8
CA50 (degATDC)	4	5	4.5	8
Swirl	1.5	1.5	1.5	1.5
Intake Temperature (C)	75	50	50	35
Intake Pressure (kPa)	115	130	130	188
ERG (%)	0	0	0	55

During CDC operation a single injection was used for all modes with the exception of mode 1 which included a small pilot injection to decrease the ignition delay of the main injection. The length and timing of the main injection was adjusted in order match the desired CA50 and load. The appendix lists the injection timing used for each case.

Table 4 Engine operating conditions for CA50 sweep

	Mode 2
Speed (RPM)	1900
IMEPg (bar)	5.7
CA50 (degATDC)	3, 5, 7, 9
Swirl	1.5
Intake Temperature (C)	50
Intake Pressure (kPa)	130
EGR (%)	0

Table 5 Engine operating conditions for swirl sweep

	Mode 2
Speed (RPM)	1900
IMEPg (bar)	5.7
CA50 (degATDC)	5
Swirl	1.5, 2.5, 3.5, 4.8
Intake Temperature (C)	50
Intake Pressure (kPa)	130
EGR (%)	0

Table 6 Fuels used for different combustion regimes

Regime	Fuel
HCCI	91PON Gasoline / n-heptane
RCCI	F76 / 91PON Gasoline
CDC	F76

Combustion Phasing Effect

A CA50 sweep was conducted on mode 2 for CDC, HCCI and RCCI. Figure 8-10 show the heat release rate, heat flux at location 3, and heat flux at location 7, for the three combustion modes respectively. The temperatures listed on the plots corresponds to the mean surface temperature for that particular case. CA50 was swept from 3degATDC to 9degATDC in 2 degree increments.

For the CDC case, as CA50 was advanced the peak heat release decreased as seen in Figure 8. Injection timings closer to TDC have shorter ignition delays and therefore a lower premixed burn fraction. Both location 3 and 7 showed advancement in peak heat flux as CA50 is advanced. Location 3 peak heat flux increases with advanced timings while location 7 does not show a trend. Location 7 is in the squish region away from the spray plumes, and was less affected by the change in injection timing.
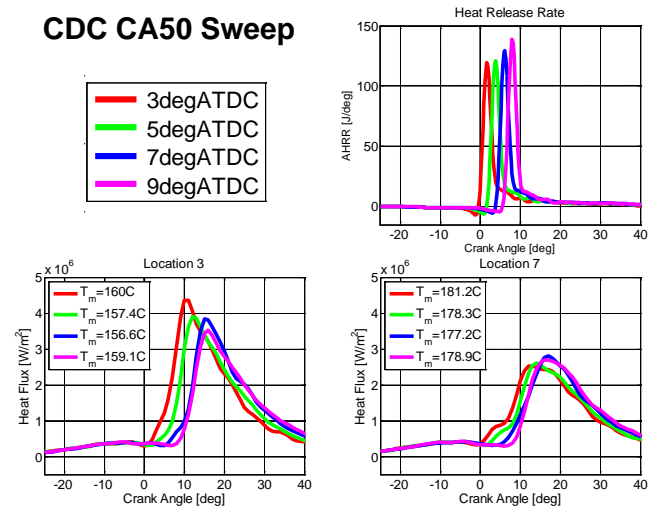

Figure 8 heat flux and heat release for CDC CA50 sweep

The HCCI data, Figure 9, are seen to be sensitive to combustion phasing. As CA50 is advanced the peak heat release rate increases and the burn duration shortens. The shorter combustion duration corresponds to an increase in PPRR. The squish land data, location 7, become similar to the CDC data at the advanced combustion phasing.
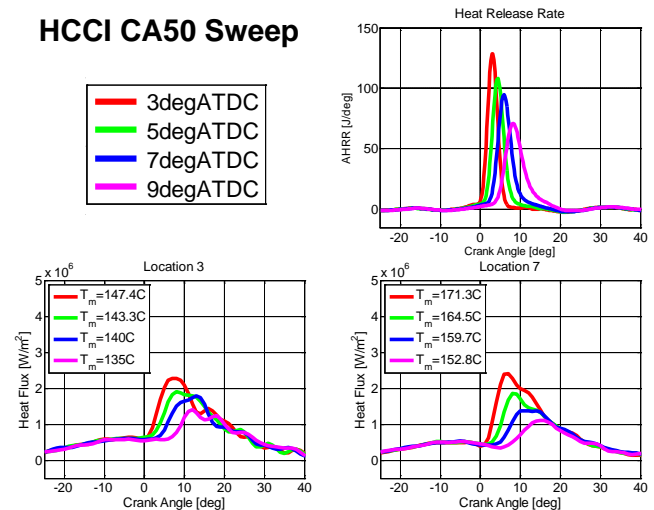

Figure 9 heat flux and heat release for HCCI CA50 sweep

The RCCI data, however, do not exhibit the same trend as the HCCI data when CA50 is changed. As seen in Figure 10, for RCCI combustion the heat release does not vary much as CA50 is advanced. The peak heat release rate increases slightly but the general shape of the heat release is unaffected by combustion phasing. The heat flux at locations 3 and 7 also remains relatively constant over the investigated range of CA50.
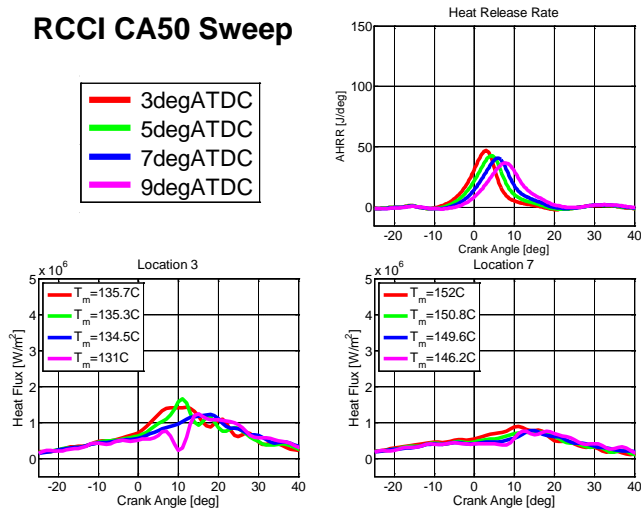
RCCI CA50 Sweep

Figure 10 heat flux and heat release for RCCI CA50 sweep

Figure 11 summarizes the effect of combustion phasing on CDC, HCCI, and RCCI by showing the peak and integrated heat fluxes. For all cases, the peak and integrated heat flux for CDC is larger, by approximately a factor of two, than for HCCI and RCCI combustion. The HCCI peak and integrated heat flux values consistently lay between the RCCI and CDC data. Location 7 peak heat flux for HCCI increases as CA50 is advanced. For the most advanced case the peak heat flux of HCCI is similar to CDC. Location 3 in the bowl region does not have as strong of a trend for HCCI as location 7.
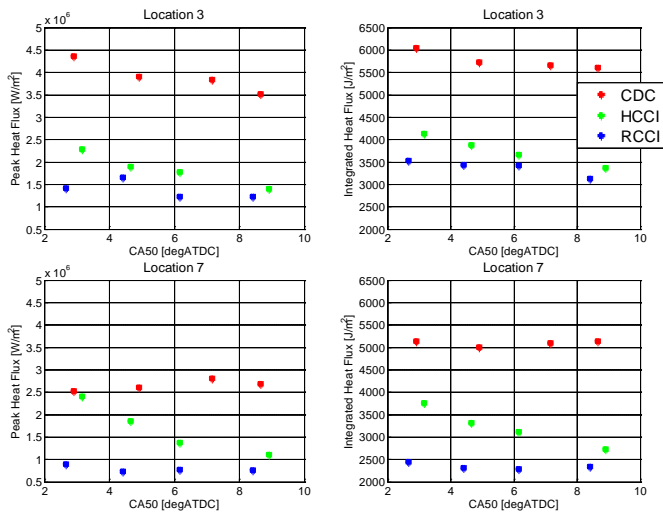

Figure 11 Integrated and peak heat flux for CA50 sweep for location 3 and 7

Swirl Effect

The swirl level was varied from 1.5 to 4.8 using the swirl control vanes mounted on the intake manifold of the engine. Figure 12-14 show the effect of swirl on CDC, HCCI, and RCCI combustion, respectively. The combustion phasing was held constant at 5degATDC for each case, and the IMEPg was

maintained at 5.7bar. The appendix shows the injection timings for CDC and RCCI.

Figure 12 shows that the heat release rate for CDC is not strongly affected by the swirl level when the CA50 is controlled. The peak heat flux at locations 3 and 7 do not show a strong trend. If one looks at the motoring part of cycle (before 0 deg), however, both locations show an increase in heat flux with increasing swirl, but the effect is much more pronounced at location 7. Because the injection timing was changed to maintain combustion phasing, it is difficult to infer how the in-cylinder fuel distribution is changing with the swirl level, e.g., where the spray plumes impact the piston. The mean surface temperature for both locations is seen to monotonically increase with increasing swirl.
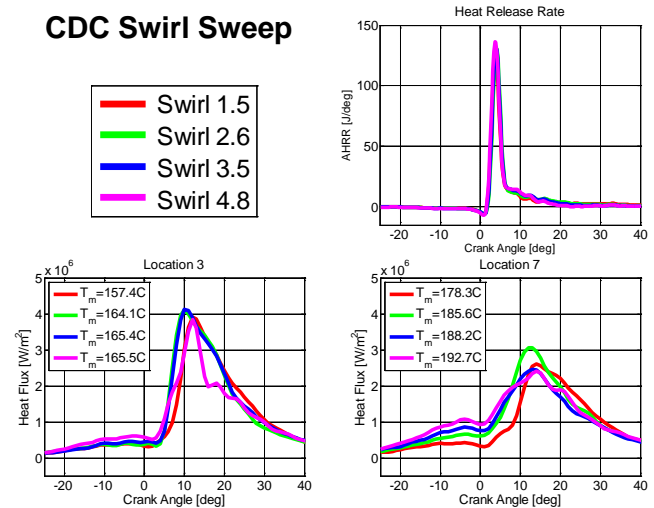
CDC Swirl Sweep

Figure 12 heat flux and heat release for CDC swirl sweep

The effect of swirl on HCCI combustion is seen to be similar to CDC. The heat flux at location 7 shows a similar increase in heat flux during compression prior to TDC as was seen in the CDC data. However, at location 3 the effect prior to TDC is not significant. There is no discernible trend seen in the peak heat flux with respect to swirl for the HCCI data. Again, as was seen for CDC, as swirl was increased the mean surface temperature also increased at both locations, suggesting an increase in the steady state component of the heat transfer.
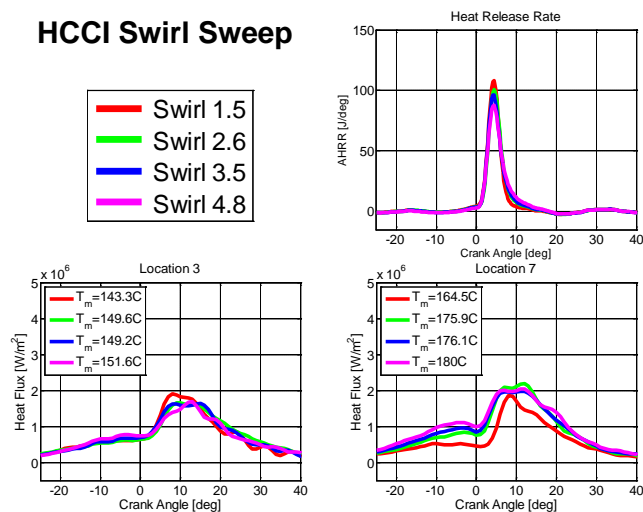
HCCI Swirl Sweep

Figure 13 heat flux and heat release for HCCI swirl sweep

As swirl increased, the peak AHRR was found to increase slightly for the RCCI combustion data, which can be attributed to the decreased gradients in reactivity because of the higher mixing rate. At location 3, the heat flux profile is largely unaffected by the swirl level. But, the mean surface temperature is seen to increase with the swirl level, suggesting a higher net heat flux to the piston. This is believed to be a result of the fact that the heat flux reported here is the dynamic heat flux. Larger differences would be expected if a backside temperature was measured and complete heat flux solution solved, as discussed above. At location 7 there is an increase in peak and integrated heat flux as swirl is increased, which is also accompanied by an increase in mean surface temperature.
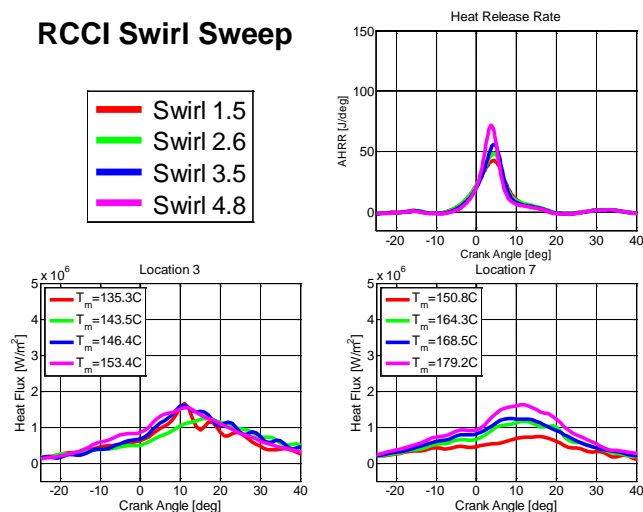
RCCI Swirl Sweep

Figure 14 heat flux and heat release for RCCI swirl sweep

Combustion Strategy Effect

To better understand the differences in piston heat transfer between CDC, HCCI, and RCCI the engine was run over a range of load and speed points. The CA50 and load were

matched for each mode in order to make a comparison. For all cases and thermocouple locations, CDC had a larger peak and integrated heat flux than HCCI or RCCI combustion. For most cases, RCCI had the lowest peak and integrated heat flux.

Mode 1 was run at 1490 RPM and 4.2 bar IMEPg as shown in Figure 15. The peak and integrated heat flux for CDC is much larger than for HCCI or RCCI combustion. The HCCI and RCCI heat flux profiles are very similar. The lower engine speed allows more time for kinetically controlled reactions to proceed. The AHRR for HCCI and RCCI are similar therefore not much difference is expected in heat flux or mean piston surface temperature.
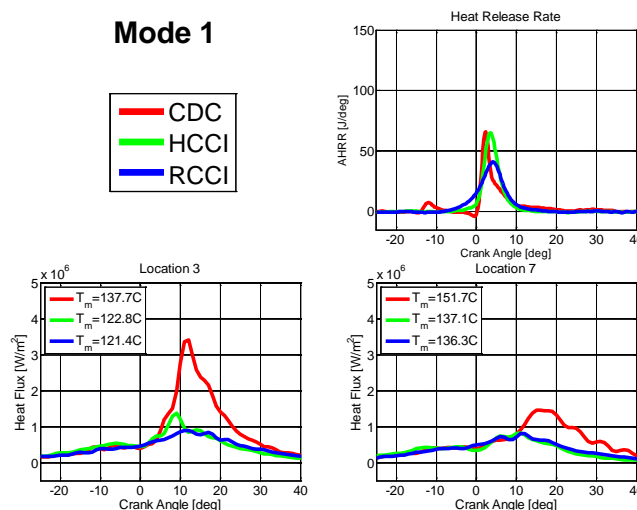

Figure 15 Mode 1 heat flux and AHRR

At mode 2, the load and speed were increased to 5.7 bar IMEPg and 1900 RPM, respectively. In Figure 16, the peak AHRR for mode 2 is much higher for HCCI and CDC than for RCCI. Although the AHRR is similar for HCCI and CDC, the heat flux is very different. The diffusion flame of CDC, with much higher local temperatures, causes the heat flux to be much greater in magnitude and duration.
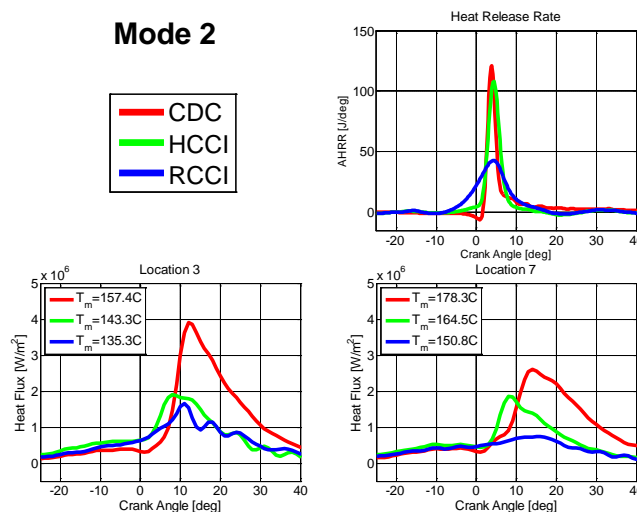

Figure 16 Mode 2 heat flux and AHRR

Figure 17 shows the mode 3 (2300 RPM and 5.7 bar IMEPg) results; the HCCI combustion event is shorter in duration than CDC and RCCI. The peak heat flux at location 3 for HCCI is greater than for RCCI but less than CDC. At location 7 the heat flux profile for HCCI begins to start to look more similar to CDC than RCCI; the peak heat flux is nearly the same in magnitude.
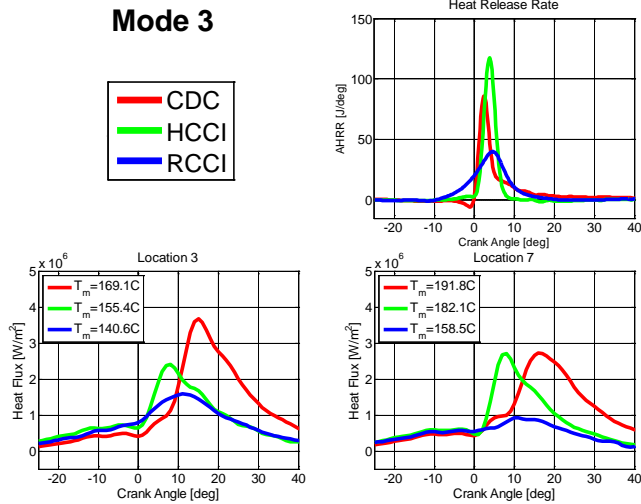

Figure 17 Mode 3 heat flux and AHRR

The mode 4 (2300 RPM and 8 bar IMEPg) results are seen in Figure 18. For this higher load point, combustion phasing was retarded to a CA50 of 8 degATDC in order to keep PPRR under control. The AHRR for HCCI shows a shorter combustion duration and increased peak AHRR when compared to RCCI, and the CDC data show a considerable diffusion-combustion tail. The heat flux at both locations is similar for HCCI and RCCI, while CDC is again larger.
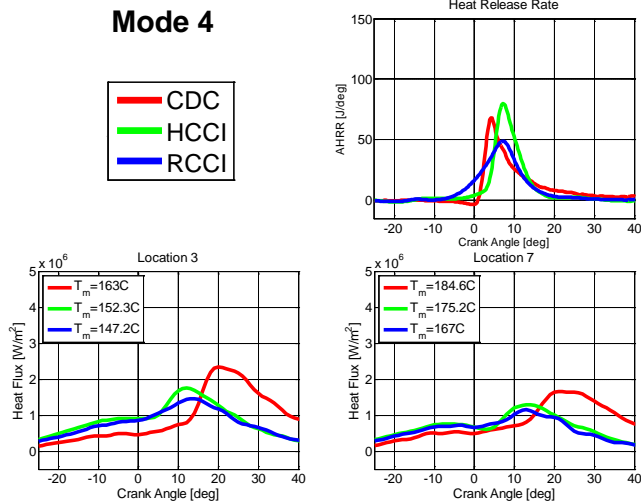

Figure 18 Mode 4 heat flux and AHRR

Figure 19 and Figure 20 summarize the integrated heat flux for the four different modes at locations 3 and 7, respectively. For all cases, CDC shows a significantly larger heat flux than HCCI and RCCI, and this is consistent with the mean surface temperatures seen in Figure 15-18. For all cases except mode

1, the location 7 RCCI case had a lower integrated heat flux than HCCI. Mode 1 was run at a lower engine speed so combustion durations for HCCI and RCCI are more similar.
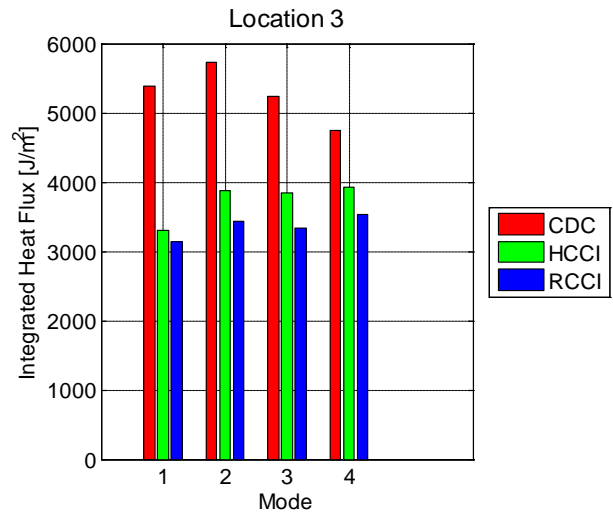

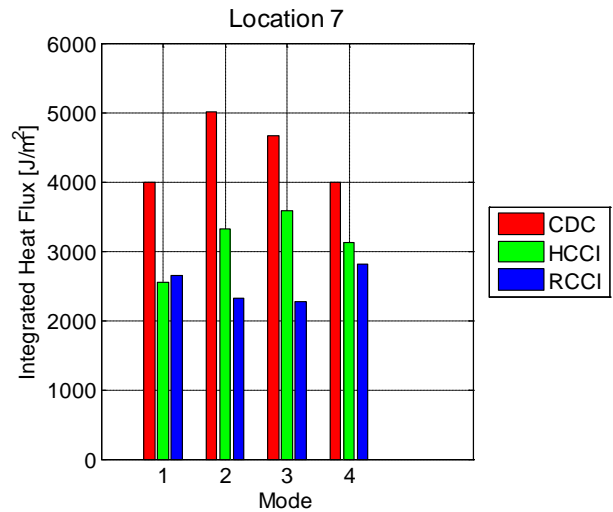Figure 19 Comparison between CDC, HCCI, and RCCI integrated heat flux at location 3

.

Figure 20 Comparison between CDC, HCCI, and RCCI integrated heat flux at location 7

Summary/Conclusions

1. RCCI and HCCI had a lower peak and integrated heat flux than CDC for all cases. The LTC strategies have lower in-cylinder temperatures than CDC, which is considered to be the main effect. Locally rich areas in CDC also lead to the formation of soot, which may also impact the heat flux; soot radiation is not expected to be present in LTC. Modeling by Kokjohn et al. discusses the origins of different heat flux for CDC and LTC and also shows similar differences [14].

UNCLASSIFIED

2. HCCI peak heat flux was similar to RCCI except for cases when the combustion duration for HCCI was significantly shorter than for RCCI, causing a violent combustion event with a high PPRR. The high PPRR events may have an effect on the piston boundary layer, causing HCCI heat flux to more closely resemble CDC.

3. An increase in swirl caused an increase in peak and integrated heat flux for RCCI and HCCI, but the trend was not as apparent for CDC. CDC is a stochastic process with directional spray plumes. Swirl may redirect the location of the plumes onto or away from the thermocouples, affecting the measured heat flux at each location. RCCI has a mostly premixed charge of air and fuel and one would expect the process to be less dependent on the location of the plumes.

4. As CA50 is advanced the peak and integrated heat flux increases for HCCI. RCCI and HCCI have similar peak heat flux for retarded CA50 but as CA50 is advanced the peak heat flux increases. The peak HCCI heat flux measured in the squish region is more strongly affected and begins to more closely resemble CDC.

References

1. Dempsey, A. B., Walker, N. R., and Reitz, R. D., "Effect of Piston Bowl Geometry on Dual Fuel Reactivity Controlled Compression Ignition (RCCI) in a Light-Duty Engine Operated with Gasoline/Diesel and Methanol/Diesel," SAE Technical Paper 2013-01-0264, 2013, doi:10.4271/2013-01-0264.

2. IR-Telemetrics. www.irtelemetrics.com, January 2013.

3. Hendricks, T., Splitter, D., and Ghandi, J., "Experimental Investigation of Pison Heat Transfer Under Conventional Diesel and Reactivity Controlled Compression Ignition Combustion Regimes," *International Journal of Engine Research (Accepted for Publication)*. 2013.

4. Miers, S., Anderson, C., Blough, J*., et al.*, "Impingement Identification in a High Speed Diesel Engine Using Piston Surace Temperature Measurements," SAE Technical Paper 2005-04-11, 2005, doi:10.4271/2005-01-1909.

5. Bendersky, D. A., "A Special Thermocouple for Measuring Transient Temperatures," *Mechanical Engineering.* 75 (2):117-21, 1953.

6. Medtherm. "Bulletin 500." 2011.

7. Rosner, B., "Percentage Points for a Generalized ESD Many-Outlier Procedure," *Technometrics.* 25 (2):165-72, 1983.

8. NIST. "Generalized ESD Test for Outliers." www.itl.nist.gov/div898/handbook/eda/section3/eda35h3.htm, October 2013.

9. Chang, J., Guralp, O., Filipi, Z*., et al.*, "New Heat Transfer Correlation for an HCCI Engine Derived from Measurements of Instantaneous Surface Heat Flux

" SAE Technical Paper 2004-01-2996, 2004, doi:10.4271/2004-01-2996.

10. Hendricks, T., Ghandhi, J., and Brossman, J., "Instantaneous Local Heat Flux Measurments in a Small Utility Engine," ASME Paper ICE2009-76035, 2009.

11. Vern Overbye, J. B., O. A. Uyehara, P.S. Myers, "Unsteady Heat Transfer in Engines," SAE Technical Paper 610041, 1960.

12. Hendricks, T., personal communication, June 2013.

13. Sasaki, S., Masuda, H., Kou, H*., et al.*, "A Transient Heat Technique for Measuring the Thermal Diffusivity of Metals," *Int. J. Thermophys.* 19 (1):259-79, 1998, doi:10.1023/A:10214115522384.

14. Kokjohn, S., Hanson, R., Splitter, D*., et al.*, "Fuel Reactivity Controlled Compression Ignition (RCCI): A Pathway to Controlled High-Efficiency Clean Combustion," *International Journal of Engine Research.* 12 (3):209-26, 2011, doi:10.1177/1468087411401548.

Contact Information

Eric Gingrich
U.S. Army TARDEC
Warren, MI
eric.m.gingrich@us.army.mil

Definitions/Abbreviations

AHRR	Apparent heat release rate		**LTC**	Low temperature combustion
ATDC	After top dead center		**NOx**	Mono-nitrogen oxides
BDC	Before top dead center		**PFI**	Port fuel injector
CA50	Crank angle at 50% to total heat release		**PM**	Particulate mater
			PON	Pump octane number
CDC	Conventional diesel combustion		**PPC**	Partially premixed combustion
EGR	Exhaust gas recirculation		**PPRR**	Peak pressure rise rate
EMF	Electromotive force		**RCCI**	Reactivity controlled compression ignition
ESD	Extreme Studentized deviate			
			RPM	Revolutions per minute
FEA	Finite element analysis		**ULSD**	Ultra-low-sulfur diesel
FFT	Fast Fourier Transform			
HCCI	Homogeneous charge compression ignition			
IMEPg	Gross indicated mean			

effective pressure